Interhemispheric Comparison of Atmospheric Circulation Features as Evaluated from NIMBUS Satellite Data

Semi-Annual Report

1 July 1973 - 31 December 1973

Grant NGR 06-002-098

DEPARTMENT OF ATMOSPHERIC SCIENCE

COLORADO STATE UNIVERSITY

FORT COLLINS, COLORADO

SEMI-ANNUAL REPORT

for

Grant NGR 06-002-098

1 July 1973 - 31 December 1973

Prepared by

E. R. Reiter, Principal Investigator

Robert F. Adler

Department of Atmospheric Science

Colorado State University

for

National Aeronautics and Space Administration

Contracting Officer: Mrs. G. Wiseman
Technical Monitor: Dr. V. Salomonson

MEAN MERIDIONAL CIRCULATION IN THE SOUTHERN HEMISPHERE STRATOSPHERE BASED ON SATELLITE INFORMATION

Robert F. Adler

Atmospheric Science Dept., Colorado State University

Fort Collins 80521

Abstract

Atmospheric structure derived from satellite, multi-channel radiance data is used to calculate zonally-averaged vertical motions in the wintertime stratosphere of both hemispheres using a heat budget approach. The Northern Hemisphere calculations based on the satellite data are shown to compare favorably with a computation carried out with conventional data, and with results of previous studies. The mean Southern Hemisphere pattern for the month of July 1969 indicates a two-celled structure with the high latitude cell centered at 60-65S. The axis of sinking motion in this cell is at approximately 50S, while the rising motion is centered at 70S. Thus the Antarctic stratospheric jet stream is associated with an indirect cell.

Two individual ten-day periods from July 1969 are examined to compare the mean meridional circulation and eddy heat flux patterns in the Southern Hemisphere during a minor midwinter warming and during a quiet period. Large eddy fluxes at 60S and a strong two-celled pattern in the meridional circulation are associated with the minor warming. During the quiet period eddy fluxes at 60S are relatively small and the mean meridional circulation appears to have a three-celled pattern with sinking motion over the South Pole.

1. Introduction

A number of studies (e.g., Vincent, 1968; Reed, Wolfe and Nishimoto, 1963; Mahlman, 1966; Julian and Libitzke, 1965) have shown that the mean meridional circulation in the lower half of the stratosphere in the Northern Hemisphere winter has a two-celled structure with rising motion in low latitudes and over the pole and sinking motion in mid-latitudes. This zonally-averaged vertical motion pattern exists before, during and after midwinter breakdowns of the polar vortex (Mahlman, 1966). In the Southern Hemisphere stratosphere the mean meridional circulation is practically unknown. Rubin and Weyant (1963) do indicate a sinking motion over the pole below 100 mb. Also Reiter (1969a, 1971) on the basis of ozone measurements over Antarctica, postulates a general sinking motion over the pole in the stratosphere. However, no calculations of the Southern Hemisphere mean meridional circulation above 100 mb have been made up to this point.

The primary reason for this absence of calculations in the Southern Hemisphere is the relative lack of radiosonde data, especially outside of Antarctica. This data problem precludes daily analysis of the stratosphere from conventional data alone, except over isolated areas. In the past few years, however, data has become available from satellite, multi-channel infrared radiometers such as the Satellite Infrared Spectrometer (SIRS) and techniques have been developed to obtain atmospheric temperature profiles from such data (see, for example, an article by Smith, Woolf and Jacob, 1970). Using such temperature retrieval techniques one can obtain daily hemispheric analyses of temperature structure at various levels. In this study temperature and geopotential height information is obtained from Nimbus 3 SIRS data.

The atmospheric structure so obtained is used as a basis for a computation of the zonally-averaged vertical motion patterns during winter months in both hemispheres. A heat budget technique is used in the calculation. The calculation is first performed using satellite-derived temperature and geopotential height information in the Northern Hemisphere for January 1970. This result is compared to another calculation based on the Northern Hemisphere gridded data fields of the National Meteorological Center (NMC), also for January 1970. The vertical motion computation is then carried out for the Southern Hemisphere with the satellite-based data fields.

2. Method used to obtain atmospheric structure from Nimbus 3 SIRS radiances

The method used in this study to obtain temperature and geopotential height information from satellite radiance data is described in detail by Adler (1974). Basically, geopotential thickness or temperature information is determined from the SIRS data by a regression technique similar to one described by Smith, Woolf and Jacob (1970). A linear, step-wise, least-squared-error, multiple regression technique is used. The dependent variables in the regression procedure are the thicknesses for the following layers: 1000-700 mb, 700-500 mb, 500-300 mb, 300-200 mb, 200-100 mb, 100-50 mb, 50-30 mb and 30-10 mb. The independent variables are the radiances of the eight SIRS channels. The weighting functions for the channels are shown in Fig. 1. Separate regression equations are determined for each layer and for each of the following latitude zones: 20-40°, 40-60° and 60-80°.

The regression technique is based on a comparison of thickness information and cloud-free radiance data. When the regression equations derived from the comparison are applied to other radiance data, only cloud-free data are used. To eliminate cloud-contaminated data from the comparison data set and from the application of the regression equations, a simple, objective "cloud check" technique is used. The "cloud check" procedure is based solely on the satellite radiance information. The SIRS channels with weighting function peaks in the low troposphere (channels 1 through 3) are most affected by the presence of clouds. Channels with weighting function peaks in the stratosphere (channels 7 and 8) are only rarely affected by the presence of tropospheric clouds. The radiance in the window channel (channel 1) in the absence of clouds

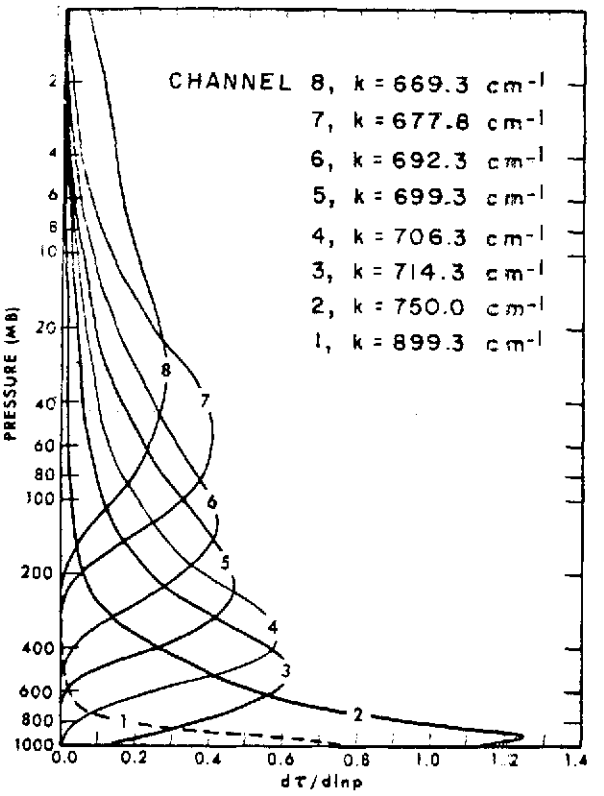

Fig. 1 Derivative of transmittance with respect to the logarithm of pressure. These functions approximately describe the relative sensitivity of the eight SIRS radiance observations to temperature variations in various altitude layers of the atmosphere (from Smith, Woolf and Jacob, 1970).

is related to the surface temperature. In the presence of an overcast, the channel 1 radiance is a function of cloud-top temperature, which is lower than the surface temperature. Therefore, channel 1 radiances much below normal would indicate the presence of clouds. However, the radiance in channel 1 is highly variable even in the absence of clouds because of its dependence on the surface temperature. Large changes in channel 1 radiance occur along satellite tracks in the presence of sharp changes in surface characteristics. This is especially true along land-sea boundaries. Also, large diurnal changes are present in the channel 1 radiance because of large changes in surface temperature. Channels 2 and 3 are also affected by clouds, but are not so severely affected by surface characteristics as channel 1. Therefore, channels 2 and 3 are used for the "cloud check."

SIRS radiance data is eliminated as being cloud-contaminated when the observed radiances in both channels 2 and 3 are below critical values. The critical values for both channels are determined by a comparison of SIRS data and satellite video data and are a function of latitude and season. Any data with both channel 2 and 3 radiances below the critical levels are eliminated as cloud-contaminated. The "cloud check" procedure is simple and certainly not foolproof. Some slightly cloud-contaminated data may still find their way into the final data set. The procedure as outlined above removes, on the average, about 15 percent of the original data points.

To obtain the regression coefficients, comparison sets of radiance and thickness data are developed. The observations are near-simultaneous and at, or close to, the same geographic position. Somewhat different techniques are used for the Northern Hemisphere and the Southern

Hemisphere. In the Northern Hemisphere, for the layer 100 to 1000 mb, the SIRS radiance data is matched with the National Meteorological Center (NMC) Northern Hemisphere fields. For satellite data occurring within three hours of NMC map time, the NMC grid point data is linearly interpolated to the satellite track position. For the layers above 100 mb, station data is matched with the satellite radiance information. The station location must be within 180 nautical miles of the satellite position, and the satellite observation time must be within three hours of the station observation time.

In the Southern Hemisphere, a different technique is used. Station data is matched with satellite radiance data for all levels. Because of the relative lack of stations in the Southern Hemisphere and the need for a sufficient number of data points for the regression analysis, the matchup restrictions are somewhat relaxed from those in the Northern Hemisphere. For each 24-hour period surrounding the 0000 GMT and 1200 GMT radiosonde times, all radiance data is placed into a five degree latitude by five degree longitude grid for the latitudes 20S to 80S. The radiance fields are analyzed and the radiances in each of the eight channels are linearly interpolated from the gridded data to the station locations. The data match-up is restricted to times and locations when there is original satellite data within a geographic box 600 nautical miles on a side surrounding the station. This technique is used for all levels.

The selection of the regression equations to be used in computing thicknesses is based on certain statistical and practical criteria. The step-wise, multiple regression technique uses an F test to determine if additional independent variables should be introduced into the particular

regression equation under consideration. In addition, the number of independent variables is restricted to a maximum of four. Most of the regression equations have three independent variables; however, a few have less than three. The standard error of estimate for each of the eight layers is given in Table 1 for each hemisphere. These statistics are for the three latitude bands combined (area weighted), and are for the dependent data on which the regression equations are based. The values in Table 1 are comparable to those in studies (e.g., Smith, Woolf and Jacob, 1970).

No regression equations could be determined for the 10-30 mb layer in the Southern Hemisphere because of a complete lack of data above 30 mb. In the analysis that follows the Northern Hemisphere 10-30 mb regression equations are applied to the Southern Hemisphere radiances to produce thickness fields in the 10-30 mb layer in the Southern Hemisphere.

	N. H. January 70	S. H. July 69
10-30 mb	2.1C	
30-50 mb	3.0	1.7C
50-100 mb	2.3	1.7
100-200 mb	2.0	1.9
200-300 mb	2.4	2.3
300-500 mb	2.8	2.3
500-700 mb	3.5	2.8
700-1000 mb	5.2	3.2

Table 1. Hemispheric standard errors of estimate for thickness regression equations

The satellite-derived thickness fields used in this study are computed by applying the regression equations to radiance data (eight channels) at 5° latitude by 5° longitude grid locations. The data are processed and placed into the latitude-longitude grid system in the following way. Each set of eight observations of radiance (there are approximately 3000 sets for each hemisphere between 20° and 80° latitude for each 24 hours) is first checked for blatant errors and then for the presence of clouds as discussed previously. If there are obvious errors or the data are determined to be cloud-contaminated, the set of observations is excluded. These two checks eliminate about 20% of the data. Each accepted set of radiances is positioned at the nearest 5° by 5° grid location. Multiple sets of data at a particular location are averaged. For each 24 hour period an average of 400 of the 936 possible locations contain original data. The remainder of the locations are filled in by linear interpolation with a greater weight placed on the east-west direction. Geopotential height information is obtained by adding thicknesses to a 1000 mb height field. This results in height data at the following levels: 700 mb, 500 mb, 300 mb, 200 mb, 100 mb, 50 mb, 30 mb, and 10 mb. In the Northern Hemisphere NMC 1000 mb height fields are used. In the Southern Hemisphere 1000 mb height analyses are obtained by converting daily surface pressure analyses of the Commonwealth Bureau of Meteorology, Australia. The Southern Hemisphere surface pressure analyses are nearly hemispheric in scope, but where they are blank the field is filled in subjectively by a combination of extrapolation and climatology.

3. Method used to calculate vertical motion

The zonally-averaged vertical motions to be presented in this study are calculated using the heat budget approach. The equation used for the calculation is derived in the Appendix.

$$\int_{\phi_1}^{\phi_2} [\omega]_\lambda \left[-\frac{\partial\theta}{\partial p}\right]_\lambda \cos\phi \, d\phi = \int_{\phi_1}^{\phi_2} \left[\frac{\partial\theta}{\partial t}\right]_\lambda \cos\phi \, d\phi + \int_{\phi_1}^{\phi_2} \left[-\frac{d\theta}{dt}\right]_\lambda \cos\phi \, d\phi + \frac{1}{a}\left\{\cos\phi_2 \left[(v_{\phi_2})_\lambda (\theta)_\lambda\right]_\lambda - \cos\phi_1 \left[(v_{\phi_1})_\lambda (\theta)_\lambda\right]_\lambda\right\} \quad (1)$$

The symbol ω represents the vertical velocity in pressure coordinates $\left(= \frac{dp}{dt}\right)$, θ is potential temperature, a is the earth's radius, v is the meridional component of the wind, λ is longitude and ϕ is latitude. The integration is over a latitude band between ϕ_1 and ϕ_2, usually 10° latitude wide.

The averaging notation used here closely follows that of Reiter (1969a, 1969b). Brackets represent an average over the coordinate given by the subscript. Parentheses indicate deviations from the mean. For example,

$$X = [X]_\lambda + (X)_\lambda \, , \quad (2)$$

where λ is longitude. The term $(X)_\lambda$ is the deviation of X from the zonal average $[X]_\lambda$. The expression $[(v)_\lambda (\theta)_\lambda]_\lambda$ is, therefore, the covariance of v and θ at one latitude or the eddy flux of θ.

The left-hand side of (1) is the temperature change due to the zonally-averaged vertical motion. The terms on the right side are respectively the local change term, diabatic heating and the temperature change due to the divergence of eddy heat flux between ϕ_1 and ϕ_2. The

terms in Eq. (1) represent the major factors in a stratospheric heat budget. The assumptions adopted to obtain (1) are described in the Appendix. It should be noted here that the horizontal heat flux related to the mean meridional circulation has been dropped. This term by itself is nearly an order of magnitude smaller than the eddy flux and also tends to be partially cancelled by a divergence term.

The local change in temperature, the static stability and the horizontal eddy heat fluxes (geostrophic) can be determined from the SIRS-derived atmospheric structure. The diabatic heating, $\frac{d\theta}{dt}$, is due to radiative heating or cooling and cannot be calculated without a knowledge of the vertical distribution of ozone. However, stratospheric, radiative heating rates, calculated from climatological conditions, are available. Rodgers (1967) has calculated radiative heating rates in the troposphere and stratosphere in the Northern Hemisphere up to 70N for the months of January, April, July and October. Similar calculations have been carried out by Dopplick (1972) between 80N and 80S for each month of the year with the results presented as cross-sections of seasonal-average values. The values of Rodgers for January appear to be almost identical to those of Dopplick for the December-January-February period in the Northern Hemisphere. Table 2 gives the values of $\frac{d\theta}{dt}$ (adapted from Dopplick, 1972) used in this study as a function of latitude and layer. The Northern Hemisphere heating rates are those given by Dopplick for the December through February period, while the June through August values are used for the Southern Hemisphere.

The calculations of $[\omega]_\lambda$ are made for each ten degrees of latitude between 40° and 80° latitude using fluxes at the intervening latitudes of 35°, 45°, etc. The computation of ω at 80° uses the flux at 75° and

the fact that the flux is zero at 90°. An additional calculation is carried out at 85° using the eddy flux at 80°.

	Latitude				
	80N	70N	60N	50N	40N
10-30 mb	-1.2	-1.2	-1.0	-0.8	-0.5
30-50 mb	-0.9	-0.9	-0.8	-0.6	-0.3
50-100 mb	-0.6	-0.6	-0.5	-0.4	-0.2
	80S	70S	60S	50S	40S
10-30 mb	-0.6	-0.8	-0.5	-0.3	-0.2
30-50 mb	-0.4	-0.4	-0.3	-0.2	-0.2
50-100 mb	-0.3	-0.3	-0.3	-0.2	-0.2

Table 2. Values of $\frac{d\theta}{dt}$ used in vertical motion calculations (Adapted from Dopplick, 1972). Units: °K day^{-1}.

4. Vertical motion patterns

The local change term in (1) is of the order of 0.1K day^{-1} while the heating due to the eddy flux convergence is of the order of 1K day^{-1} in polar latitudes. The term $\frac{d\theta}{dt}$ is negative everywhere during the polar night in the stratosphere and is of the order of 1K day^{-1}. Because the diabatic heating term varies less with latitude than the flux divergence term, the latter is most important in determining the latitudinal variability of ω. For this reason the enthalpy flux as a function of latitude is examined.

Fig. 2 shows the poleward heat flux in the 10-30 mb layer averaged over January 1970 for the Northern Hemisphere and over July 1969 for the Southern Hemisphere. Both SIRS and NMC curves are presented for the Northern Hemisphere. The geostrophic approximation is used for these computations. In both hemispheres the peak poleward flux is reached at 60°. It should be remembered that the polar vortex in the Northern Hemisphere broke down in early January that year. The two SIRS curves peak at almost the same value. The total flux convergence between 60° and the pole is approximately equal in the two hemispheres. However, the shape of the two curves is different. The Southern Hemisphere curve shows the flux decreasing very rapidly just poleward of 60S and gradually levelling out. The greatest flux convergence is in the area between 60S and 75S. The Northern Hemisphere curve has a relatively constant decrease with latitude, indicating that the flux convergence is spread out more uniformly than that in the Southern Hemisphere. This difference in shape of the enthalpy flux curves is also evident in the 30-50 mb and 50-100 mb layers, but it is not so obvious.

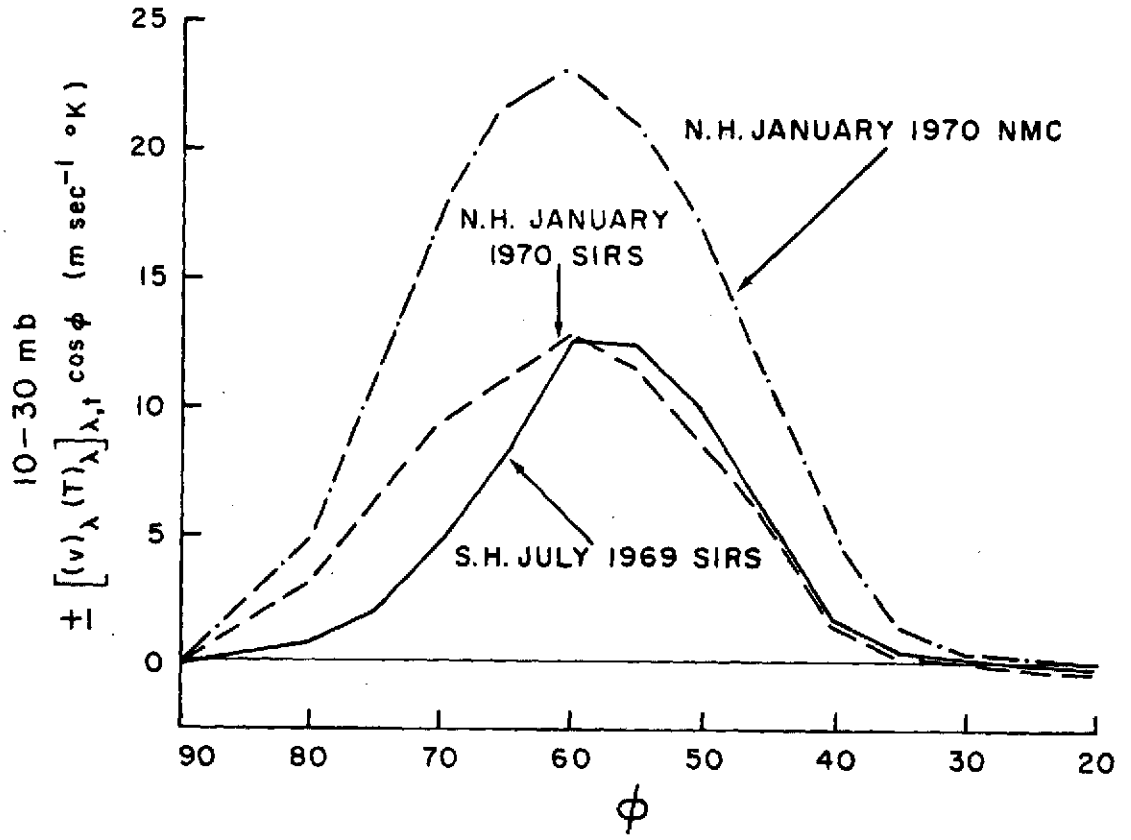

Fig. 2 Poleward heat flux in the 10-30 mb layer-January 1970 in the N. H., July 1969 in the S. H.

The enthalpy flux distributions for all three layers for the Southern Hemisphere in July 1969 are given in Fig. 3. In each layer there is a rapid decrease in the flux poleward of the peak, then a flattening out of the curve in very high latitudes. The value at 80S in the 50-100 mb layer is slightly negative, meaning that between 80S and the pole there is a flux divergence. The flux in the 30-50 mb layer at 80S has a very small positive value so that in this layer the flux convergence between 80S and 90S is also very small. In the Northern Hemisphere there is substantial flux convergence between 80N and the pole (see Fig. 2). Thus there is a significant difference between the hemispheres in the patterns of heat flux and heat flux convergence in the polar-night stratosphere.

There is also a dissimilarity between the hemispheres with regard to the relative importance of standing and transient eddies in the eddy heat flux. Here the standing eddy heat flux is calculated from the mean monthly data fields. At 60N the contribution of the standing eddies to the total flux is 79% as calculated from the NMC data and 88% as calculated from the satellite-based fields. This overestimate of standing eddy contribution is also evident in flux calculations in the troposphere (Adler, 1974). The satellite-based value at 60S for July 1969 is 65%. Judging from the Northern Hemisphere comparison this percentage is probably a slight overestimate. These percentages are for the layer 10-100 mb. Although the Southern Hemisphere standing eddy contribution is smaller, it is evident that both standing and transient eddies are important in the dynamics of the Southern Hemisphere stratosphere.

The results of evaluating the terms in Eq. (1) and solving for ω in the Northern Hemisphere for January 1970 with both NMC and SIRS-based structure are shown in Figs. 4a and b. The NMC-based calculation (Fig. 4a) shows rising motion in high latitudes and sinking in lower latitudes. The axis of ascent slopes poleward with height and the

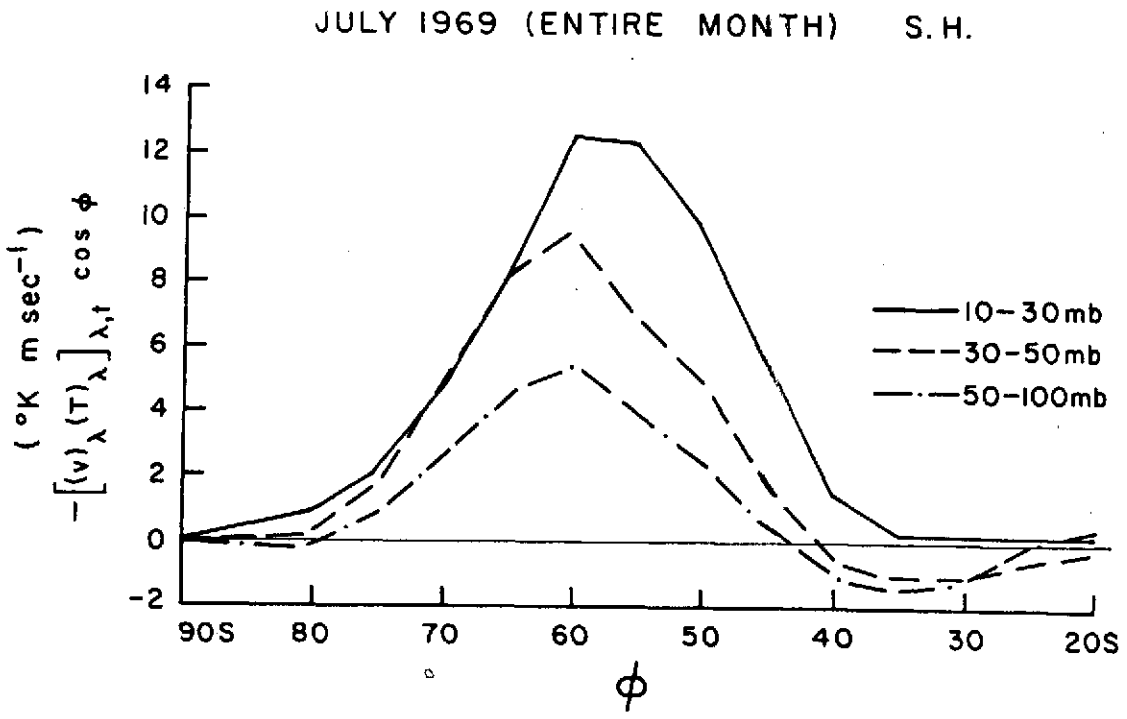

Fig. 3 Poleward heat fluxes in the stratosphere of the S. H. for July 1969.

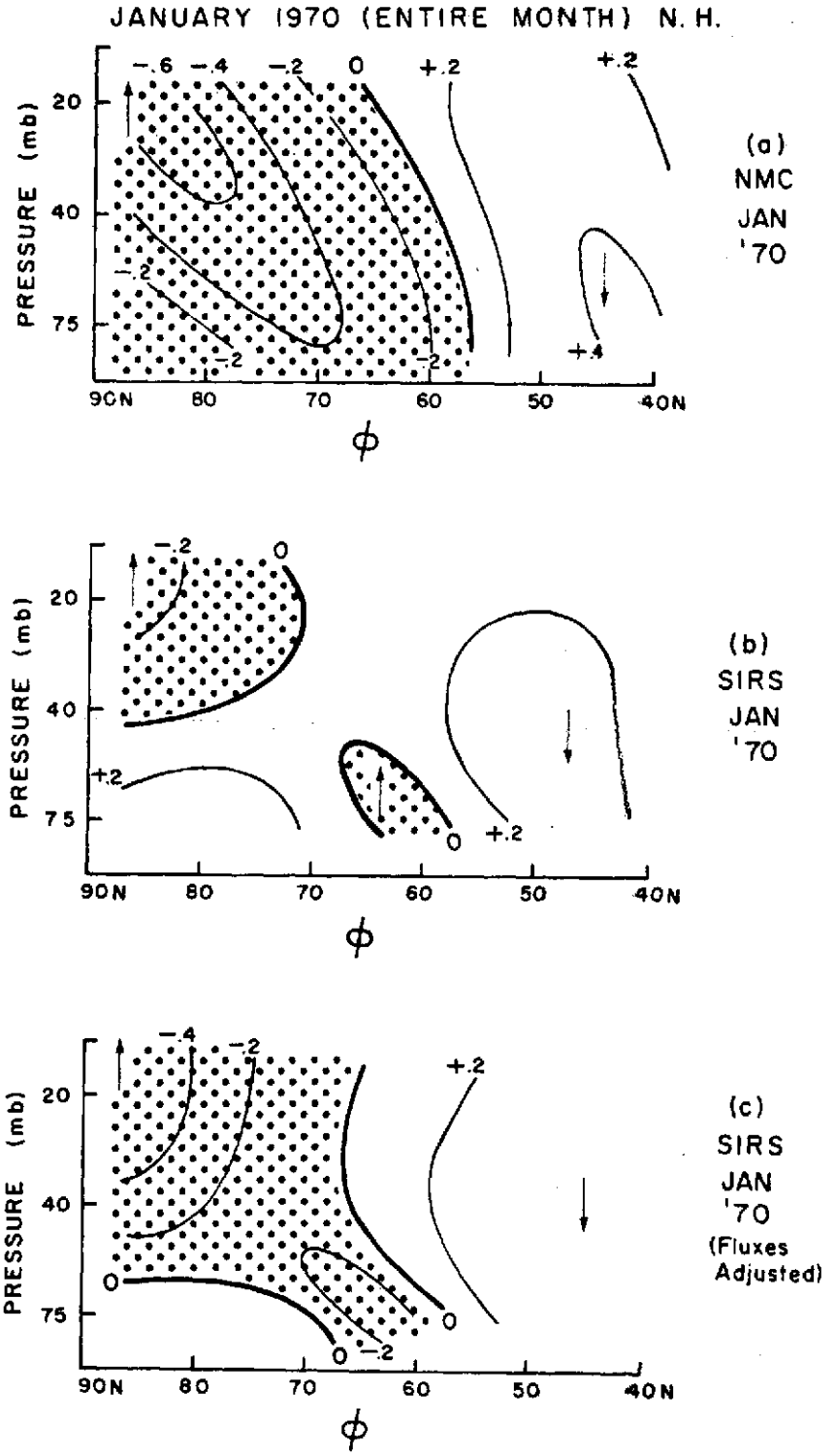

Fig. 4 Zonally-averaged vertical motion patterns for the N. H. for January 1970. Units: mb day^{-1}. Stippled area denotes area of ascent.

maximum upward motion is located at 20 mb at the pole. The pattern of rising motion over the pole and sinking in midlatitudes is typical of that found by other authors (e.g., Mahlman, 1966) for the Northern Hemisphere. Mahlman (1966) also showed that this distribution of ascent and descent occurs before, during and after breakdowns. Miller, Brown and Campana (1972) using the quasi-geostrophic, adiabatic omega equation obtain a cross-section of ω for the period 1-15 January 1970, which also indicates the same general pattern of ascent and descent as in Fig. 4a. Thus the use of Eq. (1) and NMC structure appears to produce a cross-section of vertical motion in the stratosphere which closely resembles previous estimates made for different years, and also resembles a calculation made for the same year.

The vertical velocities in this section are presented in terms of ω and in units of mb day^{-1}. The conversion from ω to $w = dz/dt$ varies with density. For a temperature of -60C the conversions are as follows for the various heights:

$$\begin{aligned} &\text{at 20 mb, 1.0 mb day}^{-1} = 3.6\text{mm sec}^{-1} \\ &\text{at 40 mb, 1.0 mb day}^{-1} = 1.8\text{mm sec}^{-1} \\ &\text{at 75 mb, 1.0 mb day}^{-1} = 1.1\text{mm sec}^{-1}. \end{aligned} \tag{2}$$

Therefore, the rising motion of 0.6 mb day^{-1} at 20 mb in Fig. 4a is approximately equivalent to 2.2mm sec^{-1}.

Fig. 4b shows the vertical motions for the Northern Hemisphere calculated using the heat fluxes, local temperature changes and static stability derived from the SIRS-based structure. There are some similarities and some differences between Figs. 4a and b. In Fig. 4b there is rising motion over the pole in the higher layers and sinking motion in midlatitudes. There is also a small area of ascent at 60N at 75 mb.

The maximum rising motion is found at or near the pole and in the top layer (10-30 mb). However, the volume of upward motion is much less than that shown in Fig. 4a. Magnitudes of maximum rising and sinking motions are underestimated.

The main factor in the difference between Figs. 4a and b is the underestimation of eddy heat fluxes in the SIRS-based calculation, evident in Fig. 2. Although the SIRS-based calculation undervalues the magnitude of the actual fluxes, it reproduces the shape of the NMC curve and the locations of flux divergence and convergence. This is also true for the two lower layers (30-50 mb and 50-100 mb). The underestimation by the SIRS-based fluxes varies with latitude and between layers, the minimum underestimation between 40N and 75N being 56%. To at least partially correct for this effect a factor of 1.8 (based arbitrarily on the 56% figure) is applied to the SIRS-based flux values and the vertical motion computation is redone. The results are shown in Fig. 4c. The general rising motion in high latitudes at high levels and the sinking motion in mid-latitudes are still present. The region of rising motion has expanded and indicates the slope with height of the NMC-based cross-section. Magnitudes of maximum rising and sinking motion are also in closer agreement. The adjustment factor 1.8 as based on the minimum underestimation is chosen because the author of this study believes that the larger underestimations present, especially in the lower layers, are due to the low density of satellite radiance data in the Northern Hemisphere for January 1970 relative to the density of observations over the Southern Hemisphere in July 1969, the Southern Hemisphere winter month to be examined.

The results of the vertical motion calculations for the Southern Hemisphere for July 1969 are shown in Figs. 5a and b. Part a of the figure is based on fluxes calculated directly from the SIRS-based structure, and part b is based on calculations made with the fluxes adjusted by the factor of 1.8. Both parts of Fig. 5 show an area of descending motion centered at 50S, an area of ascent centered at about 70S and a small area of descent over the South Pole, below about 50 mb. With the assumption of ascent in low latitudes (<30S), Fig. 5 indicates a possible three-celled meridional circulation in the lowest part of the stratosphere, and a two-celled structure in the middle stratosphere. The Southern Hemisphere pattern is significantly different from that in the other hemisphere, particularly with regard to the location and strength of the upward branch. While in the Northern Hemisphere the axis of rising motion tilts poleward in the vertical, at southern latitudes the axis is approximately vertical. The maximum rate of ascent is over the pole in the Northern Hemisphere, but is located at 70S in the other hemisphere. The magnitude of the maximum also seems to be larger in the Southern Hemisphere.

An earlier calculation of $[\omega]_\lambda$ in the Southern Hemisphere, using the diabatic heating rates of the Northern Hemisphere transposed to corresponding southern latitudes (Adler, 1973), is qualitatively very similar to the result shown in Fig. 5, except over the South Pole. Here the earlier calculation shows sinking motion up to nearly 20 mb, necessary to compensate for the larger cooling rates used (compare the values of $\frac{d\theta}{dt}$ at 80N and 80S in Table 2). The calculation presented in this paper is probably more realistic.

The boundary in Fig. 5 between the main areas of ascent and descent (60S) is the approximate latitude of the polar night jet stream. The

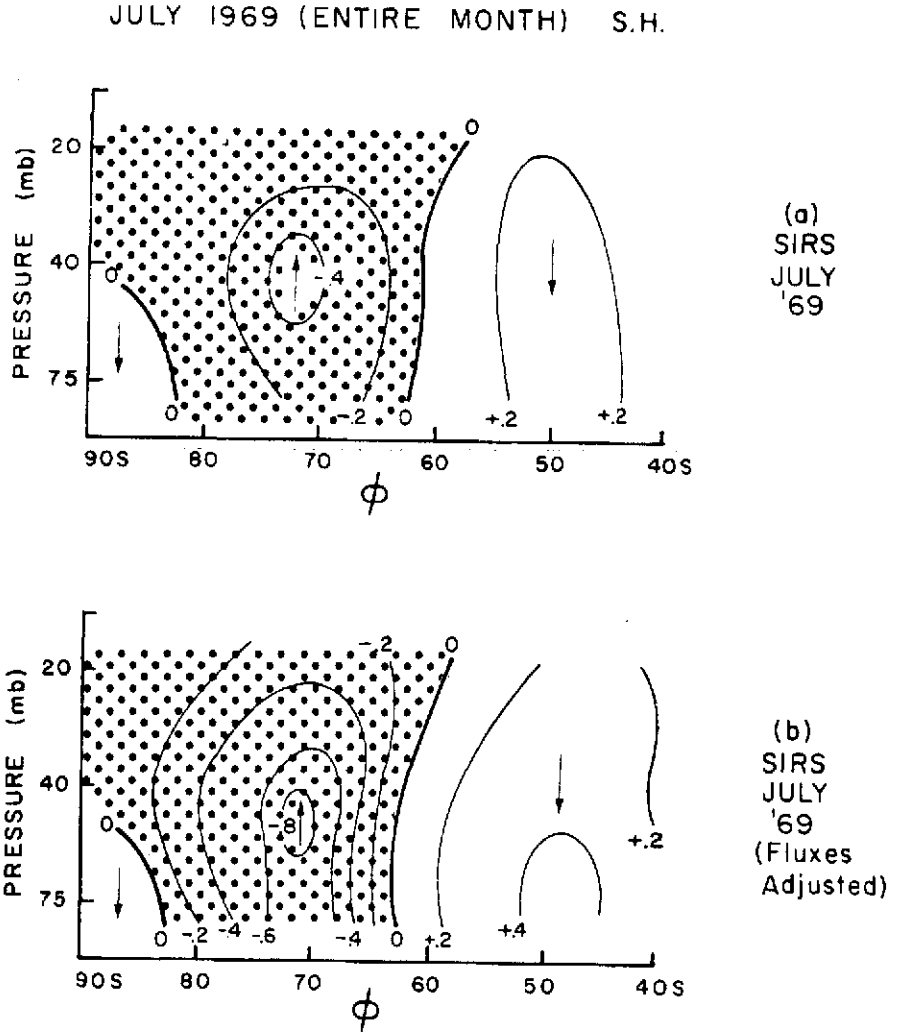

Fig. 5 Zonally-averaged vertical motion patterns for the S. H. for July 1969. Units: mb day^{-1}.

same is true in the Northern Hemisphere. Because the temperature decreases toward the pole, the mean meridional circulation around the jet stream is indirect. Therefore, there is a conversion of zonal kinetic energy (KZ) to zonal available potential energy (AZ). It seems apparent then, that the stratospheric polar jet is maintained by a conversion from eddy kinetic energy (KE) to KZ. Therefore, although mean monthly maps show a nearly zonal pattern, the eddies must still be very significant in the maintenance of the Southern Hemisphere polar night jet stream.

5. Variations in the circulation of the Southern Hemisphere stratosphere in relation to the presence or absence of a minor midwinter warming

During July 1969, there were significant variations in the circulation of the Southern Hemisphere stratosphere. These changes were related to the occurrence, early in the month, of a minor midwinter warming identified by Miller, Finger and Gelman (1970) through the use of satellite radiance data. Specifically, Miller et al. used the mean SIRS channel 8 radiance around the 60S latitude circle as a gross indicator of variations of stratospheric temperature at that latitude. This is reasonable since the weighting function (see Fig. 1) for this channel shows nearly all the contribution to the radiance coming from the stratosphere. Large increases in Miller's index are associated with a contracting of the polar vortex related to a warming event. The plot of this indicator versus time for the Southern Hemisphere winter of 1969 shows a sharp rise in mean radiance at the very end of June with a relative maximum being reached about 10 July. A very sharp decrease follows, after which there is a period of low and relatively constant mean radiance. At the very end of July, about the 29th, the mean radiance again increases sharply. The sharp rises early and late in the month are evidence of minor midwinter warmings. The period of low, relatively constant values is what will be referred to here as a quiet period. During the minor warmings at the beginning and end of July the mid-stratosphere flow was dominated by a stationary wave number 1 pattern, while the intervening quiet period was characterized by transient waves of wave number 2 (Adler, 1974).

In this section the stratospheric circulation is compared between the early July minor midwinter warming period and the following quiet period. Variations in the mean meridional motion and the eddy heat flux patterns

are examined. This early July warming is one of those studied by Fritz and Soules (1970) using SIRS channel 8 radiances. Although both Miller et al. (1970) and Fritz and Soules (1970) found significant increases in channel 8 radiance at 60S from late June to early July 1969, the major temperature increases were confined to the upper half of the stratosphere. This has already been noted by Miller, Finger and Gelman (1970) and is confirmed in the structure derived in the present study. Of the three stratospheric layers examined (10-30 mb, 30-50 mb and 50-100 mb), only the 10-30 mb layer showed a substantial rise in the zonally-averaged temperature or thickness at 60S. However, as will be seen, this does not preclude significant changes in the circulation below 30 mb.

To inspect the variability of the mean meridional circulation in relation to the presence or absence of a midwinter minor warming, calculations of zonally-averaged ω were carried out for two ten-day periods using the same method as was used for the monthly mean calculations. The first interval, 1-10 July, covers the time of the warming event. The quiet period is represented by the time span of 18-27 July. The vertical motion patterns during the minor warming and the quiet period exhibit significant differences. The vertical component of the mean meridional circulation during the minor warming is given in Figs. 6a and b. The pattern for 18-27 July 1969 (quiet period) is given in Figs. 7a and b. During 1-10 July, the area of descent over the South Pole below 50 mb disappears, and the ascending and descending branches at about 70S and 50S respectively have larger magnitudes than the monthly averages in those locations. The ascending branch is still centered between 70S and 75S.

During the quiet period (18-27 July 1969), the vertical motion pattern shows descent over the pole at all levels of this calculation (Fig. 7a

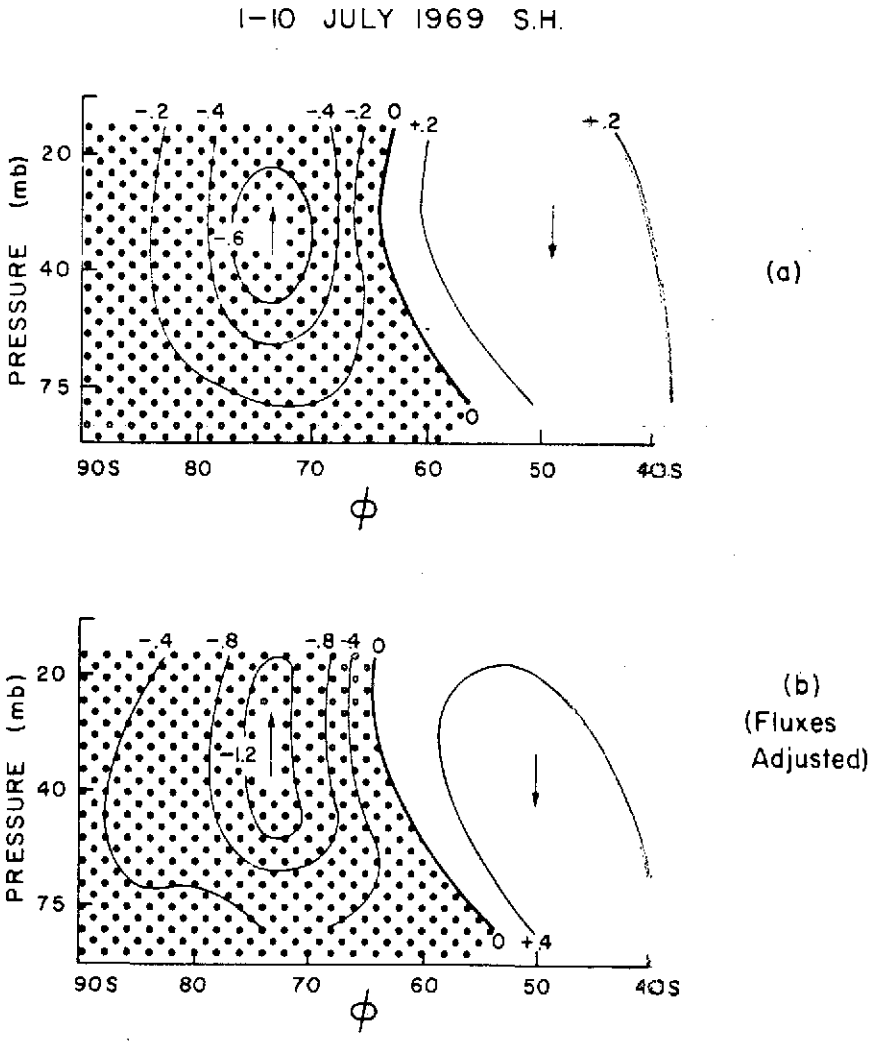

Fig. 6 Zonally-averaged vertical motion patterns for the S. H. for the period 1-10 July 1969, during a minor midwinter warming. Units: mb day^{-1}.

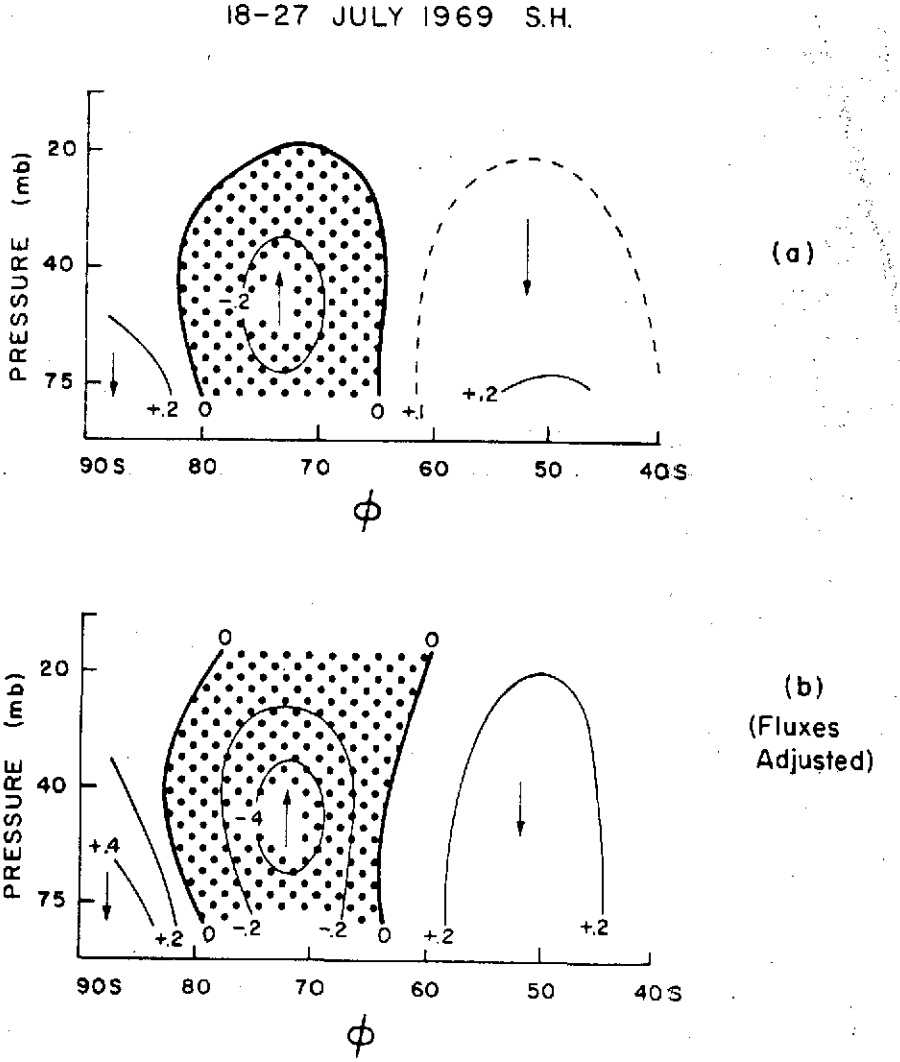

Fig. 7 Zonally-averaged vertical motion patterns for the S. H. for the period 18-27 July 1969, a quiet period. Units: $mb\ day^{-1}$.

and b). According to Fig. 7b, the descending motion covered the area poleward of about 80S with maximum downward velocity occurring in the lowest layer of calculation. Consequently, it appears that during this time period the Southern Hemisphere stratosphere has a three-celled mean meridional circulation pattern, assuming an area of ascent in low latitudes. The ascending branch at 70S and the descending branch farther equatorward are less intense than the monthly average (Fig. 5) and much less intense than they are during the minor warming (Fig. 6).

The difference in vertical motion patterns between the periods 1-10 July and 18-27 July 1969 is closely related to the eddy heat flux distributions for those two periods (see Eq. 1). These distributions are shown in Figs. 8a and b. The peak fluxes during 1-10 July are approximately three times as great as those for the 18-27 July period. Thus the flux divergences on either side of the peak are also about three times as great. In very high latitudes another important variation is that, although both the 50-100 mb and 30-50 mb layers exhibit eddy flux divergence between 80S and 90S during the period 18-27 July, all layers exhibit flux convergence in that location for the 1-10 July period. This is the reason for the calculated difference in vertical motion patterns over the pole between the two periods.

The variations with time of the heat flux and vertical motion patterns just discussed lead to some speculation concerning stratospheric events leading to the observed midwinter peaks in surface ozone observed over Antarctica (Wisse and Meerburg, 1969). During a minor midwinter warming the poleward heat flux is large and there is apparently no descending motion over the South Pole. Assuming that large heat fluxes are coincident with large poleward fluxes of ozone in the stratosphere, one may postulate

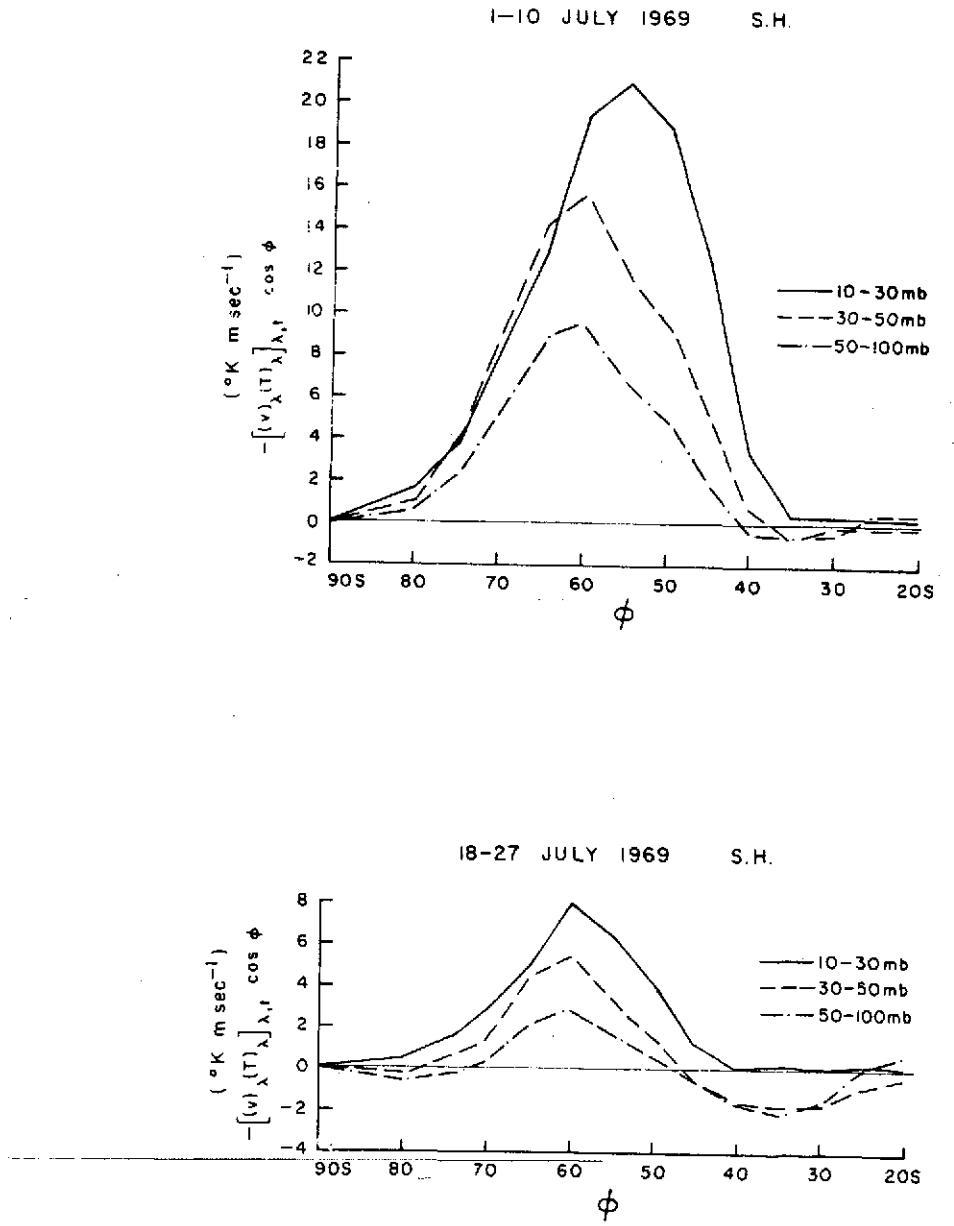

Fig. 8 Poleward heat fluxes in the S. H. during the periods (a) 1-10 July and (b) 18-27 July 1969.

a build-up of ozone in the lower stratosphere over Antarctica at that time. During an immediately subsequent quiet period the built-up ozone reservoir could be tapped by the descending motion over the South Pole which has been shown to extend through the troposphere to the surface (Rubin and Weyant, 1963).

Fritz and Soules (1970) examine a number of Southern Hemisphere stratospheric temperature fluctuations during the fall, winter and spring of 1969 using SIRS channel 8 data. As mentioned before, between 25 June and 10 July, they indicate a large increase in channel 8 radiance in the southern polar regions. Accompanying the warming (increasing radiance) in the high latitudes of the Southern Hemisphere, they also find decreasing radiance (cooling) in Southern Hemisphere low latitudes and in the Northern Hemisphere. The early July case is just one of several similar compensating changes noted by Fritz and Soules. In this section it has been noted that there are significant differences in the eddy heat flux patterns and in the derived mean meridional motion patterns between the time of the early July warming (1-10 July) and the quiet period (18-27 July). These observations support the Fritz and Soules postulate that irregular (non-seasonal) fluctuations in stratospheric temperature are related to changes in large-scale eddies and/or changes in the mean meridional circulation.

6. Conclusions

The results presented in this study indicate that atmospheric structure derived from satellite, multi-channel radiance data can be used to make reasonable estimates of important Southern Hemisphere stratospheric circulation characteristics such as the mean meridional circulation and the distribution of eddy heat flux.

The calculation of zonally-averaged vertical motion in the Southern Hemisphere stratosphere presented in Section 4 is the first realistic (that is, including the effects of eddy transports) estimate of the mean meridional circulation at those heights south of the equator. The results indicate the presence of a two-celled structure for the monthly mean pattern with rising motion centered about 70S and the axis of sinking motion occurring at approximately 50S. With temperature decreasing toward the pole in these latitudes of the stratosphere the circulation is indirect. Consequently, the Antarctic stratospheric jet stream at 60S is not maintained by the mean motions, but by the large-scale eddies.

In Section 5 there are shown to be significant variations in the Southern Hemisphere circulation during July 1969 in relation to the presence or absence of a minor midwinter warming. The mean meridional circulation during the minor warming is similar to the monthly-mean pattern; but during the quiet period the mean circulation becomes three-celled with the addition cell occurring in very high latitudes with sinking motion over the South Pole. It is possible that the quiet period may be more representative of "normal" conditions in the Southern Hemisphere stratosphere than the monthly-mean calculation. Therefore, the final determination of the normal configuration of the mean meridional circulation will have to await additional study.

Acknowledgements

This work was sponsored primarily by the National Aeronautics and Space Administration under Grant NGR 06-002-098 and also by the Atomic Energy Commission under Contract AT(11-1)-1340. The author wishes to thank Ms. Alice Fields for the computer programming.

APPENDIX

Derivation of Equation Used to Calculate Zonally-averaged Vertical Motion

The method used here to calculate the zonally-averaged vertical motion is basically a heat budget technique. The total derivative of potential temperature (θ) is expanded to give

$$\frac{d\theta}{dt} = \frac{\partial\theta}{\partial t} + \underset{\sim}{V}_p \cdot \nabla\theta + \omega \frac{\partial\theta}{\partial p} , \tag{A1}$$

where $\underset{\sim}{V}_p$ is vector horizontal wind on a surface of constant pressure, and ω is the vertical velocity in pressure coordinates. Expansion of the advection term in Eq. (A1) and a rearrangement of the terms gives

$$\left(-\frac{\partial\theta}{\partial p}\right) \omega = \frac{\partial\theta}{\partial t} - \frac{d\theta}{dt} + \nabla\cdot\underset{\sim}{V}_p\theta - \theta\nabla\cdot\underset{\sim}{V}_p , \tag{A2}$$

Next, (A2) is integrated over the area bounded by two latitudes ϕ_1 and ϕ_2, which in this study are usually 10° apart. This results in

$$\int_{\phi_1}^{\phi_2} \left[-\frac{\partial\theta}{\partial p}\omega\right]_\lambda \cos\phi \, d\phi = \int_{\phi_1}^{\phi_2} \left[\frac{\partial\theta}{\partial t}\right]_\lambda \cos\phi \, d\phi + \int_{\phi_1}^{\phi_2} \left[-\frac{d\theta}{dt}\right]_\lambda \cos\phi \, d\phi$$

$$+ \frac{1}{a}\left\{\cos\phi_2 \, [v_{\phi_2}\theta]_\lambda - \cos\phi_1 \, [v_{\phi_1}\theta]_\lambda\right\} \tag{A3}$$

$$- \int_{\phi_1}^{\phi_2} [\theta\nabla\cdot\underset{\sim}{V}_p]_\lambda \cos\phi \, d\phi ,$$

where a is the Earth's radius and $[\ ]_\lambda$ implies averaging around a latitude circle. This notation is explained in detail in Section 3.

The averaged quantities in the last two terms of (A3) are expanded to give

$$[v\theta]_\lambda = [v]_\lambda[\theta]_\lambda + [(v)_\lambda(\theta)_\lambda]_\lambda \tag{A4}$$

$$[\theta\nabla\cdot\underset{\sim}{V}_p]_\lambda = [\theta]_\lambda[\nabla\cdot\underset{\sim}{V}_p]_\lambda + [(\theta)_\lambda\ (\nabla\cdot\underset{\sim}{V}_p)_\lambda]_\lambda \tag{A5}$$

where $$[\theta]_\lambda[\nabla\cdot\underset{\sim}{V}_p]_\lambda = \frac{1}{2\pi}\,[\theta]_\lambda \int_o^{2\pi} \nabla\cdot\underset{\sim}{V}_p d\lambda \ . \tag{A6}$$

Substituting (A4) and (A5) into (A3), and using (A6) results in

$$\begin{aligned}\int_{\phi_1}^{\phi_2}\left[-\frac{\partial\theta}{\partial p}\,\omega\right]_\lambda \cos\phi\ d\phi = {} & \int_{\phi_1}^{\phi_2}\left[\frac{\partial\theta}{\partial t}\right]_\lambda \cos\phi\ d\phi + \int_{\phi_1}^{\phi_2}\left[-\frac{d\theta}{dt}\right]\cos\phi\ d\phi \\ & + \frac{1}{a}\left\{\cos\phi_2\ [(v_{\phi_2})_\lambda(\theta)_\lambda]_\lambda - \cos\phi_1\ [(v_{\phi_1})_\lambda(\theta)_\lambda]_\lambda\right\} \\ & + \frac{1}{a}\left\{\cos\phi_2\ [v_{\phi_2}][\theta]_\lambda - \cos\phi_1\ [v_{\phi_1}]_\lambda[\theta]_\lambda\right\} \\ & - \frac{1}{2\pi}\int_{\phi_1}^{\phi_2}[\theta]_\lambda \int_o^{2\pi}\nabla\cdot\underset{\sim}{V}_p \cos\phi\ d\lambda\ d\phi \\ & - \int_{\phi_1}^{\phi_2}[(\theta)_\lambda(\nabla\cdot\underset{\sim}{V}_p)_\lambda]_\lambda \cos\phi\ d\phi\end{aligned} \tag{A7}$$

In Eq. (A7), the second and third lines represent the effect of the divergence of the eddy flux and of the mean motion flux, respectively. The fourth and fifth lines represent the effect of divergence.

The last term in (A7) involves the correlation of θ and $\nabla\cdot\underset{\sim}{V}_p$. It is assumed small and, therefore, neglected. The second-to-last term is well approximated by

$$- \frac{1}{2\pi} \int_{\phi_1}^{\phi_2} [\theta]_\lambda \int_0^{2\pi} \nabla \cdot \underset{\sim}{V}_p \cos\phi \, d\phi \, d\lambda \cong - \frac{1}{2\pi} [\theta]_{\lambda,\phi} \int_{\phi_1}^{\phi_2} \int_0^{2\pi} \nabla \cdot \underset{\sim}{V}_p \cos\phi \, d\phi \, d\lambda, \tag{A8}$$

where $[\theta]_{\lambda,\phi}$ is the average potential temperature for the area between ϕ_1 and ϕ_2. The right side of (A8) is integrated to obtain

$$- \frac{1}{2\pi} [\theta]_{\lambda,\phi} \int_{\phi_1}^{\phi_2} \int_0^{2\pi} \nabla \cdot \underset{\sim}{V}_p \cos\phi \, d\phi \, d\lambda = - \frac{1}{a} [\theta]_{\lambda,\phi} \left\{ \cos\phi_2 [v_{\phi_2}]_\lambda - \cos\phi_1 [v_{\phi_1}]_\lambda \right\} \tag{A9}$$

Using the right side of (A9) to replace the second-to-last term and assuming that ω and $- \frac{\partial\theta}{\partial p}$ are uncorrelated gives

$$\begin{aligned} \int_{\phi_1}^{\phi_2} [\omega]_\lambda \left[- \frac{\partial\theta}{\partial p} \right]_\lambda \cos\phi \, d\phi = {} & \int_{\phi_1}^{\phi_2} \left[\frac{\partial\theta}{\partial t} \right]_\lambda \cos\phi \, d\phi + \int_{\phi_1}^{\phi_2} \left[- \frac{d\theta}{dt} \right]_\lambda \cos\phi \, d\phi \\ & + \frac{1}{a} \left\{ \cos\phi_2 \, [(v_{\phi_2})_\lambda (\theta)_\lambda]_\lambda - \cos\phi_1 [(v_{\phi_1})_\lambda (\theta)_\lambda]_\lambda \right\} \\ & + \frac{1}{a} \left\{ \cos\phi_2 \, [v_{\phi_2}]_\lambda [\theta]_\lambda - \cos\phi_1 [v_{\phi_1}]_\lambda [\theta]_\lambda \right\} \\ & - \frac{1}{a} \, [\theta]_{\lambda,\phi} \left\{ \cos\phi_2 [v_{\phi_2}]_\lambda - \cos\phi_1 [v_{\phi_1}]_\lambda \right\} \end{aligned} \tag{A10}$$

The last two lines in (A10) are of opposite sign and are nearly, but not quite, equal in magnitude. With a temperature gradient of 10°K/10° latitude and with θ approximately equal to 200°K, $[\theta]_{\lambda,\phi}$ is different from either θ at ϕ_1 or θ at ϕ_2 only by about 2 or 3%. The last two lines in (A10) will thus tend to cancel and their sum is negligible. Therefore, they are neglected.

The first two lines of (A10) are used for the calculation of $[\omega]_\lambda$ in this study. The first term on the right side is the local temperature change, and the second term is the diabatic heating. The third term is the temperature change due to the divergence of the horizontal eddy heat flux.

REFERENCES

Adler, R. F., 1973: Mean meridional circulation in the Southern Hemisphere stratosphere during the polar night. Atmos. Sci. Paper No. 209, Colorado State University, 25 pp.

_____, 1974: A comparison of the structure and flow characteristics of the upper troposphere and stratosphere of the Northern and Southern Hemispheres. Atmos. Sci. Paper No. 216, Colorado State University, 146 pp.

Dopplick, T. G., 1972: Radiative heating of the global atmosphere. J. Atmos. Sci., 29, 1278-1294.

Fritz, S. and S. D. Soules, 1970: Large-scale Temperature Changes in the Stratosphere Observed from Nimbus III. J. Atmos. Sci., 27, 1091-1097.

Julian, P. R. and K. Labitzke, 1965: A Study of Atmospheric Energetics During the January-February 1963 Stratospheric Warming. J. Atmos. Sci., 22, 597-610.

Mahlman, J. D., 1966: Atmospheric General Circulation and Transport of Radioactive Debris. Atmospheric Science Paper No. 103, Colorado State University, 184 pp.

Miller, A. J., J. A. Brown and K. A. Campana, 1972: A Study of the Energetics of an Upper Stratospheric Warming (1969-1970). Quart. J. R. Met. Soc., 98, 730-744.

_____, F. G. Finger and M. E. Gelman, 1970: 30 mb Synoptic Analyses for the 1969 Southern Hemisphere Winter Derived with the Aid of Nimbus III (SIRS) Data. NASA TMX-2109, Washington, D. C., 27 pp.

Reed, R. J., J. Wolfe and H. Nishimoto, 1963: A Spectral Analysis of the Energetics of the Stratospheric Sudden Warming of Early 1957. J. Atmos. Sci., 20, 256-275.

Reiter, E. R., 1969a: Atmospheric Transport Processes, Part I: Energy Transfers and Transformations. USAEC Report TID-24868.

_____, 1969b: Mean and eddy motions in the atmosphere. Mon. Wea. Rev.

_____, 1971: Atmospheric Transport Processes, Part II: Chemical Tracers. USAEC Report TID-25314.

Rodgers, C. D., 1967: The Radiative Heat Budget of the Troposphere and Lower Stratosphere. Report No. A2, Massachusetts Institute of Technology.

Rubin, M. J. and W. Weyant, 1963. The Mass and Heat Budget of the Antarctic Atmosphere. Mon. Wea. Rev., 91, 487-493.

Smith, W. L., H. M. Woolf and W. J. Jacob, 1970: A Regression Method for Obtaining Real-Time Temperature and Geopotential Height Profiles from Satellite Spectrometer Measurements and its Applications to Nimbus III SIRS Observations. Mon. Wea. Rev., 98, 582-603.

Wisse, J. A. and A. J. Meerburg, 1969: Ozone Observations at Base King Baudouin in 1965 and 1966. Arch. Meteorol. Geophys. Bioclimatol., Ser. A, 18, 41-54.

Vincent, D. G., 1968: Mean meridional circulations in the Northern Hemisphere lower stratosphere during 1964 and 1965. Quart. J. R. Met. Soc., 94, 333-349.